

Investigation of Ultrathin Ferromagnetic Films by Magnetic Resonance

Klaus Baberschke

Freie Universität Berlin, Berlin-Dahlem, Germany

1 Introduction	1617
2 <i>In situ</i> UHV-FMR: Experimental Details	1618
3 <i>g</i> -tensor and Magnetic Anisotropy Energy (MAE)	1621
4 Dynamics in the FMR, the Linewidth ΔH	1627
5 Summary, Outlook	1630
Notes	1631
Acknowledgments	1631
References	1631
Appendices	1633
A Units	1633
B Notation of the Magnetic Anisotropy Energy	1633

1 INTRODUCTION

When a magnetic dipole moment is subjected to a magnetic field \vec{H} , it experiences a torque motion. Its equation of motion is given by

$$\frac{\partial \vec{\mu}}{\partial t} = \gamma [\vec{\mu} \times \vec{H}_0] \quad \text{with} \quad \gamma = \frac{g\mu_B}{\hbar} = g \frac{(-e)}{2mc} \quad (1)$$

$$\frac{\partial \vec{M}}{\partial t} = -\gamma (\vec{M} \times \vec{H}_{\text{eff}}) \quad (2)$$

The motion of the angular momentum or the magnetic moment consists of a uniform precession about \vec{H} with angular velocity $\vec{\omega}_L = -\gamma \vec{H}$. Without damping, the component of

$\vec{\mu}$ along \vec{H} remains fixed in magnitude, so that the ‘Zeeman energy’ $E = \vec{\mu} \cdot \vec{H}$ is a constant of the motion. Real systems have a finite damping (relaxation). The dissipation of this part of energy can be pumped into the torque motion by means of microwave radiation in resonance with $\omega_{\text{MW}} = \omega_L$, yielding a Lorentzian linewidth ΔH (Figure 1b, see Section 4). Electron paramagnetic resonance (EPR) (equation 1) and ferromagnetic resonance (FMR) (equation 2) [1] are based on the same principle – for EPR see (Abragam and Bleaney, 1966; Orton, 1968; Pake, 1962), for FMR see (Vonsovskii, 1966; Heinrich, 1994; Farle, 1998). Historically, they followed very different routes: For EPR H_0 , the local and the external field are equal and known with high precision. The only unknown quantity is the *g*-factor or *g*-tensor. For FMR it is the opposite, \vec{H}_{eff} of a ferromagnet is the unknown parameter. It is the vector sum of several anisotropic field contributions (dipole, spin orbit, external, and microwave).

$$\vec{H}_{\text{eff}} = \vec{H}_{\text{dipole}} + \vec{H}_K + \vec{H}_0 + \vec{h}_{\text{MW}} \quad (3)$$

Note that the exchange field in a ferromagnet is always parallel to \vec{M} and does not contribute to the torque. \vec{M} can be seen as the sum of the individual moments per volume $\vec{M} = \sum \vec{\mu}_i$. For ultrathin simple ferromagnetic films (e.g., Fe, Co, Ni), μ is defined per particle.

In this chapter we will give a brief overview of three aspects that are most important for the investigation of novel magnetic nanostructures by means of microwave spectroscopy: The UHV-FMR technique and its monolayer sensitivity and the static parameters of magnetism (e.g., magnetic anisotropy energy (MAE) and interlayer exchange coupling (IEC), both measured with FMR in absolute energy

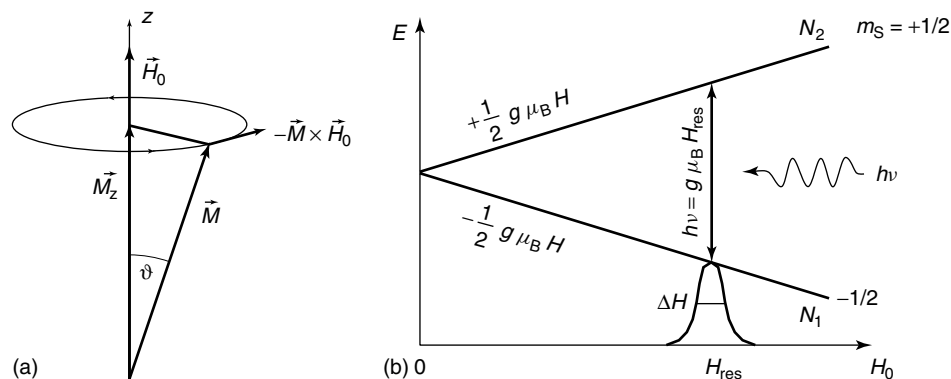


Figure 1. (a) Sketch of the uniform precession of vector \vec{M} about the external field \vec{H}_0 . (b) Zeeman levels for a spin $m_s = \pm 1/2$ system and the dipole transition for \vec{h}_{MW} being perpendicular to \vec{H}_0 .

units). Finally in Section 4 we give examples for the spin dynamics determined from the FMR linewidth.

The examples used here, mainly from our own work, will elucidate the strength of FMR and its intimate contact with *ab initio* calculations exactly adapted to FMR experiments.

2 *In situ* UHV-FMR: EXPERIMENTAL DETAILS

Magnetic resonance spectroscopy will be most instructive if external parameters can be varied. One important parameter is the temperature T . The intensity of the magnetic resonance signal (area under the resonance line) is proportional to the static susceptibility (White, 1970). Temperature variation allows us to study the EPR above the Curie temperature T_C and the FMR in the ferromagnetic phase below T_C , cf. Section 4. Other phase transitions such as those in superconductors or crystallographic phase transitions can be studied with paramagnetic impurities as a sensor by means of EPR (Baberschke, 1976; von Waldkirch *et al.*, 1973). In ferromagnets, one of the most important quantities is the MAE and its temperature dependence (Heinrich, 1994; Vonsovskii, 1966; Farle, 1998). FMR measures this directly in absolute energy units, cf. Section 3 [2]. Equally important is the measurement of the angular dependence of the resonance signal. Following equation (1), it is a standard procedure in the paramagnetic regime to determine the anisotropic magnetic moment, that is, the g -tensor (Abragam and Bleaney, 1966; Orton, 1968; Pake, 1962). If these experimental requirements can be combined with UHV, the EPR/FMR will be a very powerful experimental tool to study ultrathin ferromagnetic films. The ultimate sensitivity of microwave spectroscopy is in the range of 10^{11} spins. Usually, in standard surface science and UHV technique, molecules are adsorbed

with a submonolayer coverage onto a crystalline substrate, for example, a Cu(001) crystal. Equivalently, ferromagnetic monolayers (ML) of Fe, Co, and Ni are epitaxially grown on such a substrate with a surface area of a few square millimeters. This corresponds to $\sim 10^{14}$ lattice sites on the surfaces (Farle *et al.*, 1985). Thus the EPR/FMR should be sensitive to submonolayer coverage. This has been demonstrated for 1/100 ML of paramagnetic molecules (Zomack and Baberschke, 1986).

2.1 *In situ* UHV-FMR

Figure 2 shows the combination of a UHV chamber and a microwave EPR/FMR spectrometer. Microwave spectrometers are commercially available (Varian, Bruker). The most popular microwave frequency is 9 GHz (X band). The corresponding microwave cavity usually has a geometric size of $\sim 4 \text{ cm} \times 4 \text{ cm}$ (wavelength of the microwave $\sim 3\text{--}4 \text{ cm}$) with a central access hole of 0.5–1 in. diameter for inserting the sample. In this central access hole a quartz finger tip of a UHV chamber is inserted. In other words, the microwave cavity and all other parts of the spectrometer are operated in laboratory air. Only the sample itself is prepared and measured *in situ* under UHV conditions. This offers a very important variety of experiments, for example, to measure ultrathin films, first facing vacuum without protection layer. Then adding a cap layer and monitoring the effect of the capping on the magnetism of the ultrathin ferromagnet, or adding step-by-step *in situ* a second ferromagnetic film and studying IEC, and so on. Figure 2 shows the large electromagnet with external fields of 10–15 kOe and the field axis pointing horizontally in the laboratory frame. The sample itself is mounted on a vertical UHV manipulator with a rotating vertical axis. This allows full angular-dependent measurements varying the magnetic field from in plane to out of

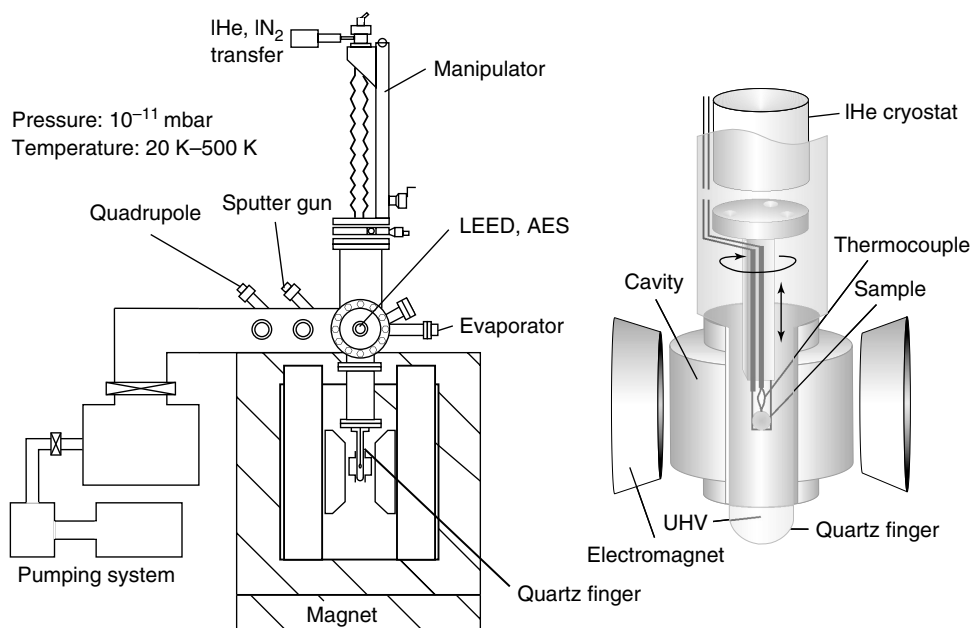


Figure 2. Sketch of the combination of a conventional EPR spectrometer with a large electromagnet and a UHV chamber equipped with all necessary installations for surface science physics (Zomack and Baberschke, 1986; Farle, 1998). The pumping station is mounted on the left-hand side, whereas the bottom part of the UHV chamber is inserted into the electromagnet and the microwave cavity. The electromagnet (being movable on a track) and the microwave cavity are taken away from the UHV chamber for a standard bakeout procedure to reach a base pressure in the 10^{-11} mbar range. For details see text.

plane. The commercial manipulator is equipped with a cooling system for ℓHe or ℓN_2 . It has a very large z (vertical) travel of ~ 50 cm. This specialty is necessary to move the sample above the electromagnet into the upper part of the UHV chamber for sample preparation. This upper level is equipped with standard surface science UHV instruments such as Auger, LEED, quadrupole, evaporator, sputter gun, and so on. Recording a typical FMR spectrum takes only a few minutes. Thus, a full angular dependence or temperature dependence may be measured within an hour. Afterward, the sample may be moved to the upper position for further sample preparation such as adding a cap layer or a second ferromagnet, adsorbing gas on the surface, and so on. Finally it is moved down again for a second *in situ* experiment.

Figure 3 shows the EPR/FMR of Gd/W(110) as one example. The Curie temperature of bulk Gd equals $T_{\text{Cb}} \approx 292$ K, for 1.6 ML Gd/W(110) it is $T_{\text{C}} < 292$ K (open squares) due to the finite size effect. Figure 3(b) convincingly shows the high sensitivity of the FMR. At 316 K, the signal for 1.6 ML is recorded with a very good signal-to-noise ratio. The resonance signal has been monitored from 360 K to below the corresponding Curie temperature for each film (Farle and Baberschke, 1987). The steep increase of the intensity follows the temperature dependence of the susceptibility of the Gd films. The external field \vec{H}_0 was applied in plane along the easy axis of the Gd film. Consequently, the external resonance field shifts to lower values at lower

temperature because the internal one $\vec{H}_{\text{dipole}} + \vec{H}_{\text{K}}$ increases when the temperature is reduced.

The idea of a fingertip inserted into a microwave cavity has been used before for $^3\text{He}/^4\text{He}$ dilution refrigerators (Nagel *et al.*, 1980; Baberschke and Tsang, 1980). The same idea of experimental setup, namely, the combination of UHV technique with magnetic measurements can be used to determine the magnetization with a SQUID (Ney *et al.*, 2002) as well as the ac-susceptibility χ_{ac} (Stetter *et al.*, 1992). All three techniques FMR, SQUID, and χ_{ac} combined with state-of-the-art surface physics and UHV technique offer a new insight into the understanding of the fundamentals of the magnetism of ultrathin ferromagnetic films.

2.2 Multifrequency FMR

Following equation (1), we estimate that a typical resonance condition is given for ~ 10 GHz and ~ 3.5 kOe. Under certain limitations the absorption of electromagnetic waves between two Zeeman levels is proportional to ω^2 . Thus EPR microwave spectroscopy is more sensitive by ~ 4 orders of magnitude than nuclear magnetic resonance operating in the range of 100 MHz. On the other hand, microwave spectroscopy has some limitations. It operates usually only at one fixed frequency due to microwave oscillators and the waveguide technique. Consequently, the magnetic field has

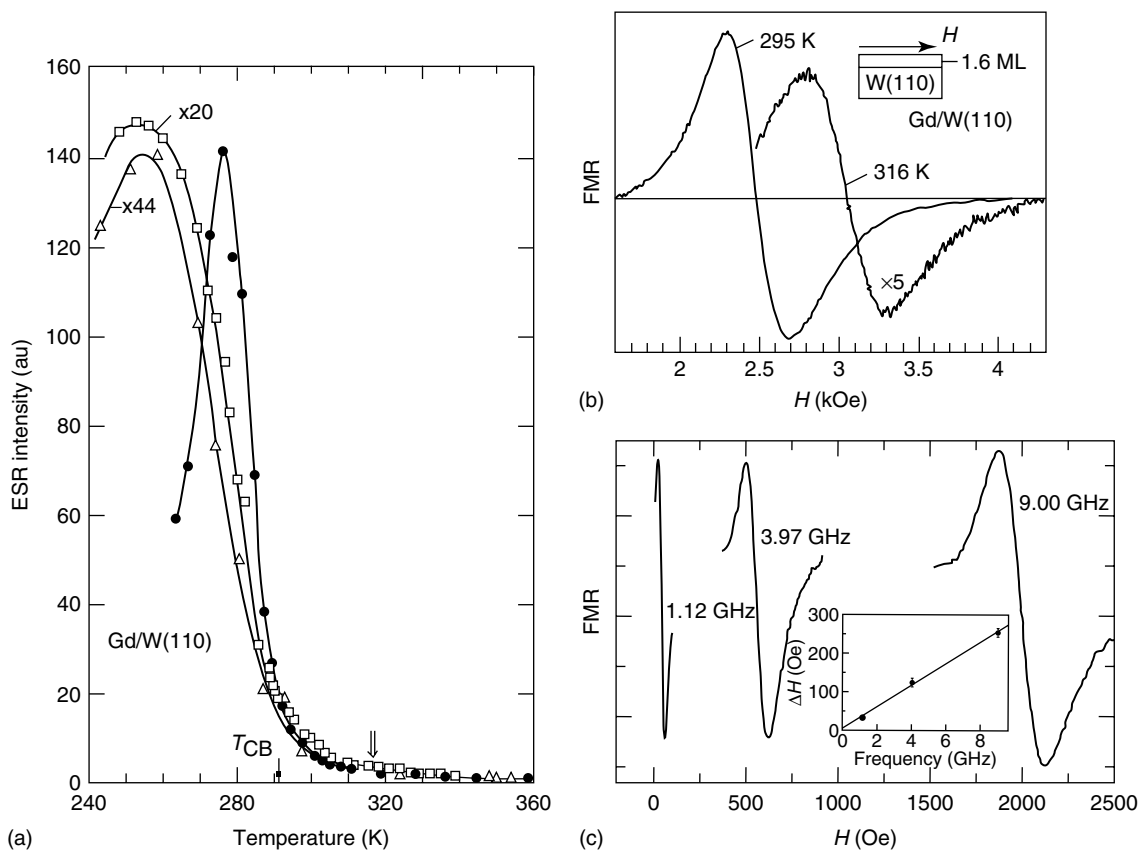


Figure 3. Typical magnetic resonance spectra of ferromagnetic monolayers (Farle and Baberschke, 1987). (a) EPR intensity for different film thickness: 80 Å (full circles), 1.6 ML (open squares), 0.8 ML (open triangles). The arrow at 316 K corresponds to the experimental spectrum given in (b). Note that the spectrum at 295 K in (b) is still above T_C . (c) FMR of 7 ML Ni/Cu(001) at 1, 4, and 9 GHz. The spectra are taken in the ferromagnetic phase. Corresponding to equations (1) and (2) also the external Zeeman field reduces if the microwave frequency is reduced. Note the narrowing of the linewidth – at 1.12 GHz the linewidth is $\Delta H = 15$ Oe only (cf. Section 4). All three spectra are taken *in situ* in UHV without protective layer for the same film, just by replacing the microwave cavities.

to be scanned (see Figure 1b). The majority of experiments are performed in dilute paramagnetic systems. These experiments focus mostly on the determination of the different components of the g -tensor (equation 1). Consequently, the larger the frequency, the better the separation of different components of the g -tensor (slopes in the Zeeman level) for a given linewidth. Field scanning in a ferromagnetic film creates some difficulties. First of all, in contrast to a paramagnet, the ferromagnet has an internal anisotropy field with an easy and a hard axis in the crystallographic frame. Thus, the applied external field and the internal field are usually not collinear. Scanning the external field through the resonance condition means, in principle, dragging the magnetization behind the field direction and, as a consequence, the Lorentzian line shape should be deformed. Fortunately, this effect is very small. More important is the analysis of the measured linewidth itself. If determined at only one frequency, it will not be so easy to interpret this value. In the past, quite frequently some inhomogeneous broadening

assuming local field distribution was used for the interpretation of the width. In Figure 3(c) we show the FMR of 7 ML Ni/Cu(001) at 1, 4, and 9 GHz. Obviously, the linewidth is strongly frequency dependent and narrows down to a few oersteds only at low frequencies. This means that frequency-dependent measurements are very important to disentangle relaxation processes and other contributions to the linewidth of the FMR in ultrathin ferromagnetic films. Fortunately, microwave cavities in this lower frequency range (1, 3, 4 GHz) are available with the same geometrical size as the 9 GHz cavity and the same central access hole of 1 in. diameter. This allows us to keep the sample in UHV, only replacing the 9 GHz microwave cavity by a 1 or 4 GHz cavity, and measure the same film. In Section 4 it will be shown that FMR measurements at very high frequencies of 200 GHz and more are also of relevance to investigate the dynamics of magnetic nanostructures. For these frequencies, the wavelength reduces to below the millimeter regime. Different experimental techniques are needed (Silsbee *et al.*, 1979;

Monod and Janossy, 1977). Currently these experiments are not performed in UHV. Here, one still needs a protective cap layer to record the FMR signal.

3 g-TENSOR AND MAGNETIC ANISOTROPY ENERGY (MAE)

To solve the equations of motion equations (1) and (2) under the influence of a small oscillatory microwave field \vec{h}_{MW} with $\vec{h}\tau \perp \vec{H}_0$ and to calculate the resonance condition with ω_{MW} and a given external magnetic field H_0 we refer to standard literature, for example, (Vonsovskii, 1966; Heinrich, 1994; Farle, 1998). It is the advantage of magnetic resonance spectroscopy that the method to calculate the resonance condition and interpret, for example its angular dependence (direction of H_0 with respect to the crystallographic axis of ultrathin films), is well established for a long time. In this section we give a few examples to demonstrate the power and usefulness of FMR to gain information on the intrinsic parameters of ultrathin ferromagnetic structures. The resonance conditions are given below for the polar and azimuthal angular dependence

$$\begin{aligned} \left(\frac{\omega}{\gamma}\right)^2 = & \left[H_0 \cos(\theta - \theta_H) \right. \\ & + \left(-4\pi M_{\text{eff}} - \frac{2K_{2\parallel}}{M} + \frac{K_{4\perp}}{M} - \frac{K_{4\parallel}}{2M} \right) \cos 2\theta \\ & + \left. \left(\frac{K_{4\perp}}{M} + \frac{K_{4\parallel}}{2M} \right) \cos 4\theta \right] \times \left[H_0 \cos(\theta - \theta_H) \right. \\ & + \left(-4\pi M_{\text{eff}} - \frac{2K_{2\parallel}}{M} + \frac{K_{4\parallel}}{M} \right) \cos^2 \theta \\ & + \left. \left(\frac{2K_{4\perp}}{M} + \frac{K_{4\parallel}}{M} \right) \cos^4 \theta + \frac{2K_{2\parallel}}{M} - \frac{2K_{4\parallel}}{M} \right] \quad (4) \end{aligned}$$

$$4\pi M_{\text{eff}} := 4\pi M - 2K_{2\perp}/M \quad (5)$$

and for $\theta = \theta_H = 90^\circ$:

$$\begin{aligned} \left(\frac{\omega}{\gamma}\right)^2 = & \left[H_0 \cos(\varphi - \varphi_H) + \frac{2K_{2\parallel}}{M} \cos 2(\varphi - \varphi_u) \right. \\ & + \left. \frac{2K_{4\parallel}}{M} \cos 4\varphi \right] \times \left[H_0 \cos(\varphi - \varphi_H) + 4\pi M_{\text{eff}} \right. \\ & + \left. \frac{2K_{2\parallel}}{M} \cos^2(\varphi - \varphi_u) + \frac{K_{4\parallel}}{2M} (3 + \cos 4\varphi) \right] \quad (6) \end{aligned}$$

where θ_H is the polar angle of the external magnetic field H_0 with respect to the surface normal of the thin film, θ the angle of the magnetization, and φ the azimuthal angle in plane.

Only along the easy and hard axis of the magnetization, the vectors \vec{M} and \vec{H}_0 are parallel and $\theta = \theta_H$. For all other orientations, the equilibrium angle of θ can be calculated by minimizing the free energy of the system (Smit and Beljers, 1955). Full angular-dependent measurements of the FMR of ultrathin films have shown in numerous cases the dragging of the magnetization, see for example, Figure 38 in (Farle, 1998). Equations (4)–(6) also show the various contributions of anisotropy fields K_i/M (Berghaus *et al.*, 1989). In several cases, the analysis of the experimental results was projected on two mechanisms only as given in equation (5): The dipole or shape anisotropy field $4\pi M$ and the so-called uniaxial out-of-plane anisotropy contribution $K_{2\perp}/M$, also called K_u/M . However, equations (4) and (6) show that full angular-dependent FMR measurements also give access to $K_{2\parallel}$. An axial in-plane symmetry is usually caused by steps at the surface or can be observed for vicinal crystal surfaces. Since many of the ultrathin ferromagnets (Fe, Co, Ni) are grown pseudomorphically on nonmagnetic single-crystal substrates like Cu or GaAs, they will not grow in their bulk crystallographic cubic structure but will be tetragonally or trigonally distorted. This can easily be detected by monitoring the $K_{4\perp}$ and $K_{4\parallel}$ contributions – K_4 is a fourth-order term but in most cases not of cubic symmetry. For details of the MAE and its notation, see Appendix B.

As stated in the introduction one focal point of FMR investigations in the past was the determination of anisotropy energies and anisotropy fields in ultrathin ferromagnets. It was often assumed that the g value is close to $g = 2$ for the free electron (Vonsovskii, 1966; Heinrich, 1994). In contrast, equations (4) and (6) offer the opportunity to determine not only anisotropy fields but also, independently, the proper g value as is common practice in standard EPR. Resolving the double parentheses product in equation (4), we see that there exists one term that depends only on the external magnetic field H_0^2 . FMR experiments at different frequencies offer the possibility of determining g also from the proportionality of the parabolic behavior of $\omega^2 = f(H)$. This will be discussed in the following subsection.

3.1 g-tensor, μ_L , μ_S

In the past it was often assumed that the orbital magnetic moment is quenched in cubic Fe, Co, and Ni structures and magnetism was explained in terms of the spin magnetic moment only. However, giant orbital magnetic moments have been observed recently in magnetic nanostructures (Gambardella *et al.*, 2003). Even in bulk cubic materials, the survival of large orbital moments for itinerant magnets has been observed (Brewer *et al.*, 2004). Kittel (Meyer and Asch,

1961) has already shown that the departure from $g = 2$ is a measure of the ratio of orbital-to-spin magnetic moment [3].

$$\frac{\mu_L}{\mu_S} = \frac{g - 2}{2} \quad (7)$$

For bulk Fe, Co, and Ni, the g value increases from 2.09 to 2.21 (Stearns, 1986). This tells us that in Ni μ_L is already 10% of the spin moment, and μ_L is parallel to μ_S in accordance with the positive sign of the spin-orbit coupling constant. In EPR, it is also well known that the light 3d elements like Cr have g values $g < 2$, the spin-orbit constant is negative and μ_L and μ_S are aligned antiparallel. EPR/FMR have the capability to measure orbital and spin magnetism. As a matter of fact, standard second-order perturbation theory (Abragam and Bleaney, 1966; Orton, 1968; Pake, 1962) shows that the MAE and the anisotropy of the orbital magnetic moment are caused by the same matrix elements mixing excited states into the magnetic ground state.

One example in thin-film magnetism is given in Figure 4. A thick Fe film and ultrathin Fe_n/V_m multilayers were measured by two techniques: FMR and X-ray magnetic circular dichroism (XMCD) (Anisimov *et al.*, 1999). For the same specimen, the ratio of the orbital-to-spin magnetic moment was measured by both techniques. In Figure 4(a), the ratio is given as function of the Fe thickness. A thick Fe film of 40 nm shows $g = 2.09$ corresponding to $\mu_L/\mu_S = 0.045$. When reducing the Fe thickness to 4 and 2 MLs only, the g value increases up to $g = 2.26$, which means an increase of μ_L by a factor of 3. In Figure 4(b), the XMCD spectra for both, the V and Fe $L_{3,2}$ edges are plotted. It is known that at an Fe/V interface a magnetic moment is induced at the V site. Following Hund's rule for V (Fe) spin and orbital moment are antiparallel (parallel) aligned. This leads to an enhancement of the effective orbital moment and a

reduction of the total spin moment. FMR measures the total magnetic response of such a multilayer structure, whereas X-ray absorption spectroscopy (XAS) and XMCD (see also **Synchrotron Radiation Techniques Based on X-ray Magnetic Circular Dichroism, Volume 3** and **Magnetic Spectroscopy, Volume 1**) are element-specific methods and are, therefore, in a position to measure the magnetism at the Fe and the V site separately as shown in Figure 4(b). The apparent discrepancy between the determination of μ_L/μ_S by FMR and XMCD can therefore easily be explained. XMCD (full circles) measure only the Fe contribution. For the total response as probed by FMR we note from Figure 4(b) that the spin moment of V is antiparallel to that of Fe. The total spin moment is reduced. In contrast, the orbital moments of Fe and V are aligned parallel. Therefore, the larger value for the ratio (open circles) determined by FMR is completely understandable.

In conclusion, owing to its element-specificity, XMCD measures μ_S and μ_L at the Fe and the V site separately. FMR determines the ratio μ_L/μ_S from the g value. If a second measurement, for example by SQUID, provides the total magnetization ($\mu_L + \mu_S$), spin and orbital contributions may be separated without XMCD.

3.2 MAE in a ferromagnetic monolayer

The *in situ* FMR in ultrathin Ni/Cu(001) films of 3–25 ML has been used to study the spin reorientation transition (SRT) (Schulz and Baberschke, 1994). To analyze the experimentally determined K values properly it is important to notice that when changing the thickness of the ferromagnetic film, the Curie temperature T_C will change, too. It is therefore not advisable to plot $K(1/d)$ at a fixed thermodynamic temperature T but rather at the reduced temperature $t = T/T_C$.

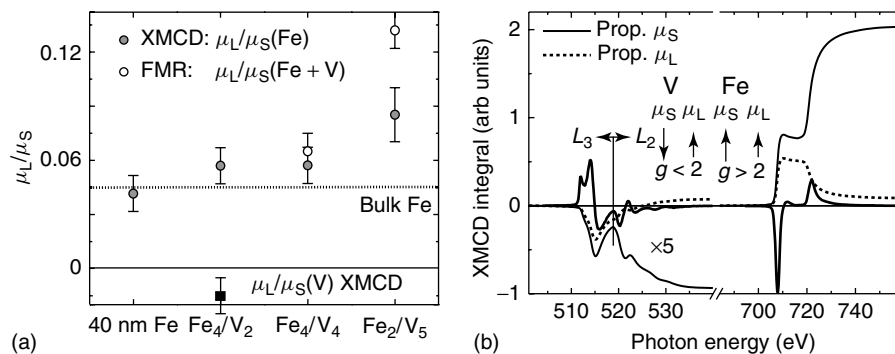


Figure 4. Orbital and spin magnetic moments, μ_L and μ_S , respectively, of Fe/V multilayers measured by FMR and XMCD (Scherz *et al.*, 2001). (a) The ratio μ_L/μ_S increases with decreasing Fe thickness. Note that XMCD measures only the Fe moments (full circles), whereas FMR measures the total (Fe and V) response (open circles). The ratio μ_L/μ_S of V in Fe_4V_2 as obtained from XMCD (full squares) is negative because μ_L and μ_S are aligned antiparallel in V. (b) XMCD spectra (thick solid line) and integrated XMCD signals as they would appear in the spin (thin solid line) and orbital (dotted line) sum rule.

Comparing experimental results only makes sense if the data are taken at the same reduced temperature. The MAE vanishes at T_C , that is, it is zero in the paramagnetic regime. In Figure 5(a) two sets of data are plotted: full circles at $t = 0.56$ and open triangles at $t = 0.74$. That this is an important point is seen in Figure 5(b) in which experimental data are plotted at a fixed temperature of $T = 300$ K as a function of the thickness from ~ 1 to ~ 10 ML. At first glance, it seems that as the film becomes thinner the anisotropy K increases with a positive slope. If, however, the data of Farle *et al.* (1999) (full circles) are plotted at a fixed, reduced temperature $t = 0.21$ (Figure 5c) instead of a fixed absolute temperature $T = 300$ K, again a linear function of $1/d$ results with negative slope up to ~ 6 ML. This is the only correct way of analyzing magnetic anisotropy of ultrathin films. Figures 5(a) and 5(c) can be interpreted in the same way: Starting from right to left, at very thin films of ~ 3 ML we see a linear increase with negative slope of $f(1/d)$ up to a particular value of ~ 15 ML for Ni and ~ 6 ML for Co. In the ultrathin limit, the Ni and Co films grow pseudomorphically with tetragonal distortion for Ni(001) (trigonal for Co(111)). At the bending, the pseudomorphic growth stops and the films grow in the natural bulk structure of the specific material, for example, fcc for Ni. These linear dependences of $K(1/d)$ in Figure 5(a) and 5(c) confirm equation (A3), namely, the classical argument by Néel that the surface and interface anisotropies scale down with $1/d$. The diagrams also show the extrapolation of the linear slope to the y axis indicated as K^V . Let us assume for sake of argument that ultrathin films of Ni or Co grew with a rigid perturbed lattice structure (i.e., tetragonally distorted owing to pseudomorphic growth) up to infinite thickness, indeed an extremely large volume anisotropy of 30 or 90 $\mu\text{eV}/\text{atom}$ would occur. Of course, ferromagnetic films do not do that. The growth mode collapses back to the natural bulk lattice structure of the material with much lower anisotropy per particle. We did

observe that this linear function and bending in $K(1/d)$ is the most sensitive indicator for changes in the growth mode. The crystallographic structure may change only by less than 0.1 \AA , which is difficult to measure by diffraction (LEED) but does have large effects on MAE and K .

FMR measures the total M_{eff} (equation (5)). After subtraction of the dipole contribution $2\pi M^2$, the K parameters (Figure 5) can be plotted as a function of $1/d$ or as a function of T (for details see Appendix B). We also see that $2\pi M^2$ has to be scaled with the reduced temperature. It is obvious that because of the small magnetic moment per Ni atom the shape anisotropy for Ni is much smaller ($\sim 10 \mu\text{eV}/\text{atom}$) than for Co ($\sim 90 \mu\text{eV}/\text{atom}$) with a large magnetic moment per atom. This is the simple reason why the easy axis of magnetization for ultrathin ferromagnetic films of Co is in most cases in plane. Whereas for Ni the K anisotropy caused by the spin-orbit coupling can exceed the dipole contribution and result in an SRT from in plane to out of plane at ~ 7 – 9 ML (e.g., Figure 5a). For details see (Baberschke 1996, 2001; Farle, 1998). Like in bulk ferromagnets, the various K_i parameters have a different temperature dependence. For bulk, see (Stearns, 1986), for ultrathin films, see (Farle, 1998; Baberschke, 2001). In equations (4) and (6) the shift of the external resonance field H_0 as a function of the temperature or angle is measured in absolute field units, that is, Oe. For a given magnetization, this can easily be translated into energy units. Many other spectroscopies discussed in this volume measure magnetic anisotropy usually only in arbitrary units. Determining the absolute MAE is the strength of the FMR. Therefore, a new challenge is to compare FMR experiments with *ab initio* calculations from first principles.

The importance of the temperature dependence of the MAE in ferromagnetic nanoclusters recently became very evident. Various groups have investigated small ferromagnetic particles (e.g., Co) by means of MOKE and XMCD, measuring very large MAE and orbital magnetization.

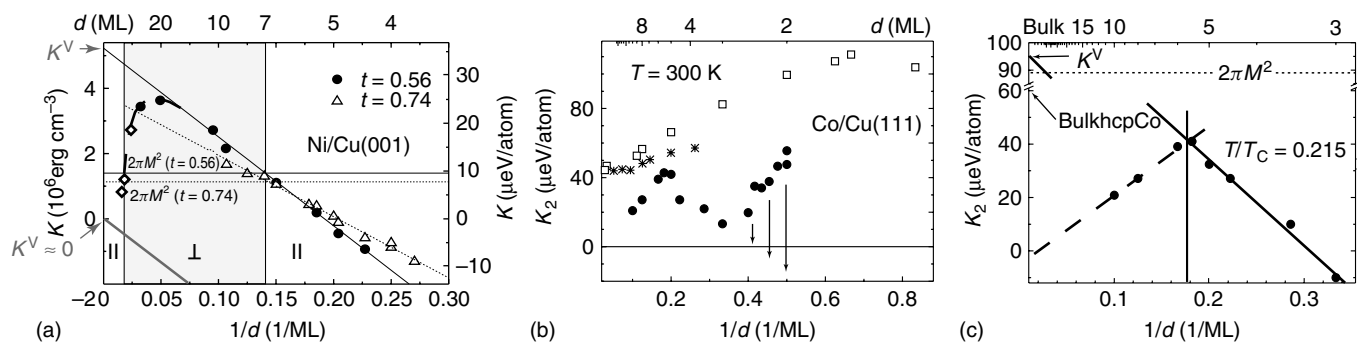


Figure 5. K_2 anisotropy as a function of $1/d$ (a) for Ni/Cu(001) at different reduced temperatures (Schulz and Baberschke, 1994), (b) and (c) for Co/Cu(111). The data in (b) are taken from (Huang *et al.*, 1994) (open squares) and (Kohlhepp *et al.*, 1993) (asterisks). Both were measured at fixed, ambient temperature. The data taken from (Farle *et al.*, 1999) (full circles) are plotted at fixed temperature in (b) and as a function of reduced temperature in (c).

Usually, one assumes a uniaxial anisotropy constant K_u . However, Antoniak *et al.* (2005) measured the temperature dependence $K(T)$ for Fe/Pt nanoparticles with FMR and observed that it changes between 50 and 300 K by one order of magnitude. This explains the whole magnetic behavior of these nanoparticles.

To demonstrate the high sensitivity of the MAE on small crystallographic lattice perturbations, we show in Figure 6(a) *ab initio* calculations for an infinite-sized single Ni crystal. It is an all electron, full relativistic calculation including orbital polarization (full symbols) and without orbital polarization (open symbols). The infinite-sized crystal was chosen to demonstrate the importance of the volume contribution K^V . K^V is defined as the difference in total energy between the hard and easy axis, for bulk Ni the [100] and [111] magnetization directions (Hjortstam *et al.*, 1997). The difference in total energy was calculated for different ratios c/a , starting from an fcc lattice ($c/a = 1$), passing through a regime with tetragonal symmetry and ending in a bcc symmetry ($c/a = 1/\sqrt{2}$). For fcc and bcc, K^V almost vanishes, $K^V \ll 1 \mu\text{eV}/\text{atom}$. In the tetragonal regime, K^V increases by orders of magnitude up to $K^V \approx 500 \mu\text{eV}/\text{atom}$. For the FMR experiments shown in Figure 5, the pseudomorphic growth of the Ni film produces a constant ratio $c/a \approx 0.95$ (gray regime in Figure 6a). The *ab initio* calculations in Figure 6 yield an anisotropy energy of $K^V \approx 100 \mu\text{eV}/\text{atom}$. This result is in perfect agreement with the experimental finding after extrapolating the experimental value to $K^V(T = 0)$.

Comparing experiment and theory, one comes to the conclusion that *changes in the nearest-neighbor distance of $\sim 3\%$, that is, $\sim 0.05 \text{ \AA}$, may change the MAE by orders of magnitude.*

The Weinberger group (Uiberacker *et al.*, 1999) has performed similar calculations for a particular FMR experiment on a 12 ML Ni film grown on a Cu substrate and facing vacuum. Figure 6(b) shows the magnetic part of the difference in total energy per individual Ni layer. For the open triangles, a rigid, unrelaxed fcc lattice was assumed, whereas open squares and open circles are calculations for a relaxed tetragonal Ni structure adapted to the lattice of the Cu substrate. It is obvious that the topmost Ni layer facing vacuum shows a large negative contribution corresponding to the negative slope in Figure 5(a). It is also clear that the first Ni layer on the Cu substrate has a different (smaller) negative energy contribution due to hybridization with the Cu band structure. Such an effect cannot be separated in an FMR experiment – the experiment measures the sum of the two contributions. However, the center part of the 12 ML Ni film is most instructive: For a rigid cubic lattice, their energy contribution is very small. If, however, one puts the real relaxed lattice as determined from experiment into the calculation, we see that the center part of an ultrathin film also contributes to the total MAE in full agreement with the results of Figure 6(a). That is to say, *surface and interface magnetic anisotropy contributions K^S are certainly very large following the early argument by Néel, but they usually count only*

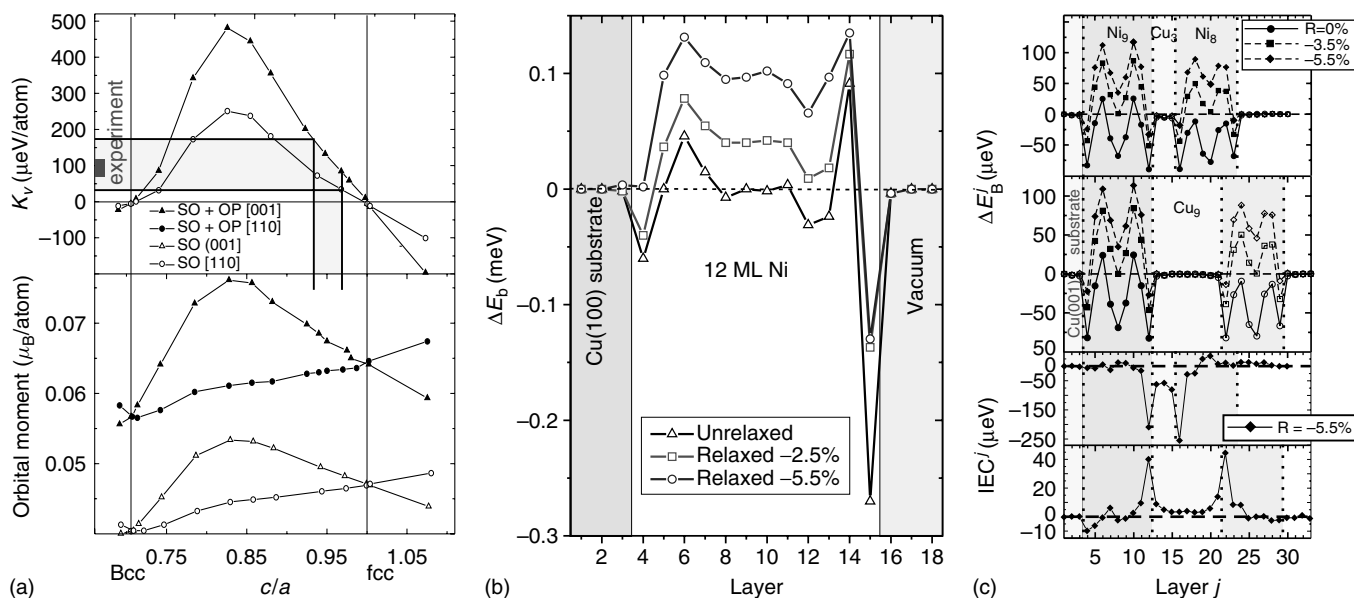


Figure 6. *Ab initio* calculations of MAE and IEC for various Ni structures. (a) The difference in total energy is calculated for an infinite-sized Ni crystal as a function of the ratio c/a . (Taken from Hjortstam *et al.*, 1997.) The lower part shows the orbital moment and its anisotropy. (b) Similar *ab initio* calculations for a 12 ML Ni film, layer resolved. (Taken from Hjortstam *et al.*, 1997.) (c) Similar calculations for a trilayer also showing the IEC, see Section 3.3. (Taken from Hammerling *et al.*, 2003.)

for one layer each, whereas the central part of an ultrathin film counts for $n - 2$ layers. For the particular example shown here, it is obviously clear that the K^V contribution to the total MAE is the dominating one. For the details of the nomenclature, see Appendix B.

3.3 UHV-FMR in a trilayer and interlayer exchange coupling (IEC)

The archetype of a magnetic multilayer structure is the so-called ‘trilayer’, consisting of two FM films, FM1 and FM2, weakly exchange coupled via a nonmagnetic spacer NM. Two exchange-coupled ferromagnetic films exhibit two eigenmodes of the uniform motion of the magnetizations M_1 and M_2 – like two coupled pendula. Analogous to the notion of phonon branches, they are labeled acoustic (in phase) and optic (π out of phase) modes. The FMR is the technique of choice for investigating these spin-wave dynamics (Lindner and Baberschke, 2003b). It measures both AFM and FM coupling and determines the MAE and IEC parameters. For such a case, \vec{M} has to be replaced by the vector sum $\vec{M}_1 + \vec{M}_2$ in the equation of motion, equation (2).

Furthermore, an additional energy contribution of the IEC energy is added to the free-energy density. Following the FMR resonance condition, equations (4–6) also have to be modified. One has to distinguish the individual anisotropy parameters of each FM film, for example, K_i^{Ni} and K_i^{Co} (for details see (Heinrich, 1994; Lindner and Baberschke, 2003a)). In theoretical calculations, the IEC usually enters with an IEC constant at $T = 0$. Most of the experiments are analyzed with an effective parameter J_{inter} .

$$F_{\text{ex}} = -J_{\text{inter}} \frac{\vec{M}_1 \cdot \vec{M}_2}{M_1 M_2} \quad (8)$$

The scalar product $\vec{M}_1 \cdot \vec{M}_2$ takes care of the individual orientation of M_i in each film. (Note that in an FMR experiment with an external magnetic field H_0 , the orientation of M changes as a function of the orientation and strength of H_0 .) In Figure 7, an instructive example is given showing that in a step-by-step experiment the UHV-FMR gives detailed information on all relevant magnetic parameters for such trilayers.

Figure 7(a) and (b) show the experimental and simulated FMR spectra of a $\text{Ni}_7/\text{Cu}_9/\text{Co}_2$ trilayer at two different

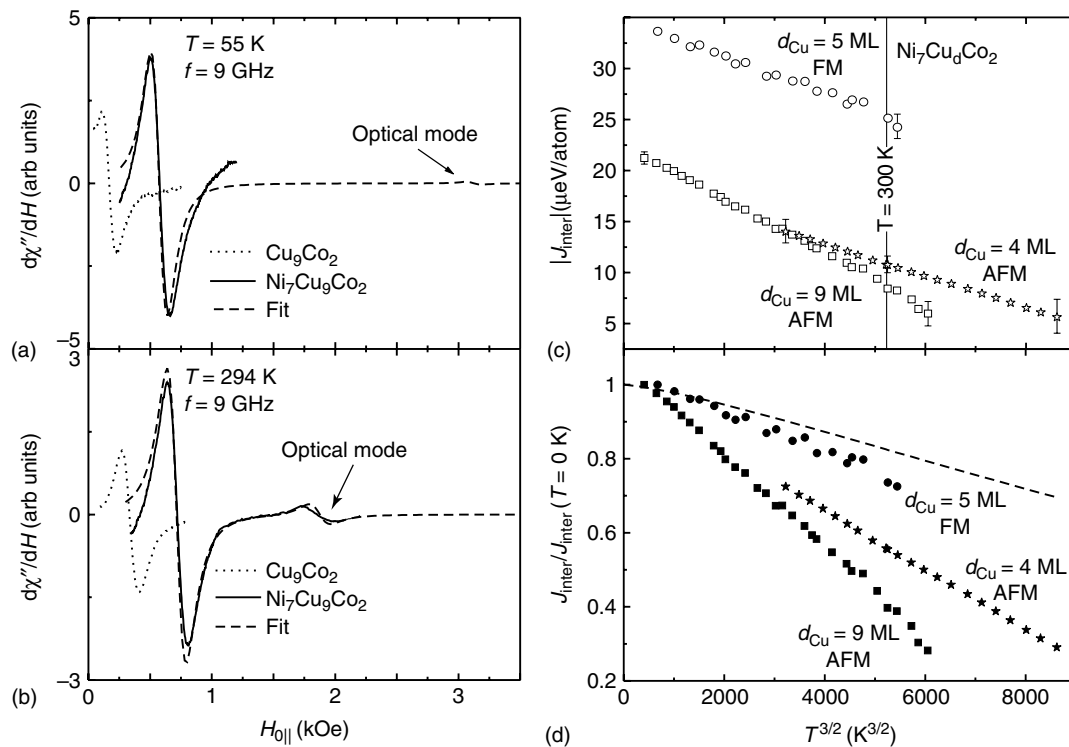


Figure 7. (a) and (b) experimental and calculated FMR spectra of a Ni/Cu/Co trilayer at different temperatures along the in-plane easy axis, taken from (Lindner *et al.*, 2002). First the single Co film on Cu(001) was measured (dotted). Subsequently the top Ni film was evaporated. The same type of experiment was carried out for different spacer thicknesses d_{Cu} for AFM and FM coupling. J_{inter} determined from the FMR fitting is plotted in absolute energy units in (c) and normalized to $T = 0$ in (d) as a function of an effective $T^{3/2}$ law (Schwieger *et al.*, 2007).

temperatures. First, only the Co₂ film capped with the Cu₉ spacer layer was prepared. A single resonance line (dotted) is recorded. Its intensity and position change because K_i and M are temperature dependent. In a second step, the Ni₇ film is deposited on top. At room temperature, the FMR records two resonance lines: one of the weak optical mode and a second one of the strong acoustical mode. From the intensity and position of the two lines it is immediately evident that this trilayer has an AFM coupling between the two ferromagnetic films (Heinrich, 1994; Lindner and Baberschke, 2003a). The simulation of the coupled resonance lines (dashed) is in perfect agreement with experiment. A full measurement of the dependence on the polar angle and the temperature gives access to all MAE parameters, provided $M(T)$ is known from another experiment. Taking the angular dependences of only the bottom film and the IEC trilayer, all unknown parameters influencing the resonance field of the optical and acoustical mode can be determined. The only parameter left, which determines the resonance shift, is J_{inter} itself. This straightforward way of determining the coupling demonstrates the advantage of *in situ* measurement. The coupling between FM1 and FM2 is an oscillatory function of the spacer thickness (Bruno and Chappert, 1991). For the particular system Ni₇/Cu_d/Co₂, this has been observed and determined by UHV-FMR for a spacer thickness in the range of $d_{\text{Cu}} = 2\text{--}9$ ML (Lindner and Baberschke, 2003a). Again, it is documented in textbooks (Heinrich, 1994) that FMR is equally applicable for AFM and FM coupling: for AFM coupling, the intense acoustical mode appears at a lower magnetic field than the weak optical mode; for FM coupling, this reverses such that the optical mode is at a lower magnetic field than the acoustical mode. We note that FM1 and FM2 in trilayers may also consist of the same material, for example, Ni₈/Cu_d/Ni₉. For Ni films of different thicknesses, the MAE values and magnetization are different, leading to different eigen resonances of the individual modes.

Another important parameter for understanding the magnetism of coupled ferromagnetic films is the *temperature dependence* of the coupling strength, that is, $J_{\text{inter}} = f(T)$. Two models were proposed in the past:

1. Thermally excited spin waves in the magnetic layers lead to a reduction of the effective IEC. In this model, the characteristic temperature is given by T_C . Arias and Mills calculated a $T^{3/2}$ power law (Arias and Mills, 1999, 2000):

$$\frac{J_{\text{inter}}}{J_{\text{inter},0}} = 1 - a \left(\frac{T}{T_C} \right)^{3/2} \quad (9)$$

Other parameters like the thickness of the spacer layer are hidden in the prefactor a .

2. In the framework of electronic band structure, the smearing of the Fermi edge at elevated temperature makes the coupling less effective, excitations of electron–hole pairs reduce the IEC (Bruno, 1995). This temperature-dependent factor was calculated by Bruno as given in equation (10).

$$\frac{J_{\text{inter}}}{J_{\text{inter},0}} = \frac{T/T_0}{\sinh\left(\frac{T}{T_0}\right)} \quad (10)$$

The characteristic temperature T_0 is controlled by electronic band structure effects, that is, v_{Fermi} and the spacer thickness. The Curie temperature is no explicit parameter but is implicitly included via the intralayer coupling of the ferromagnets.

Lindner *et al.* (2002) have shown for various ultrathin film systems over the full temperature range from ~ 0 K up to T_C that the effective temperature dependence is very close to the $T^{3/2}$ law and can be less well fitted by a $x/\sinh(x)$ function. However, Nolting and coworkers (Schwieger and Nolting, 2004; Schwieger *et al.*, 2005) have reinvestigated the origin of the temperature dependence of the IEC yielding an effective functional dependence, which for given intra- and interlayer exchange parameters gets very close to an effective exponent of $\sim 3/2$ but does not follow the exact power law for spin-wave excitations with $T^{3/2}$. For the Ni₇/Cu_d/Co₂ trilayer system, the temperature dependence is plotted in Figure 7(c) and (d). Figure 7(c) gives the absolute values for $|J_{\text{inter}}|$. For $d_{\text{Cu}} = 5$ ML the coupling is FM, for $d_{\text{Cu}} = 4$ ML and $d_{\text{Cu}} = 9$ ML the coupling is AFM. In Figure 7(d) the measured values are normalized to $T = 0$, this eliminates the temperature-independent part of $|J_{\text{inter}}|$. Nonmonotonic slopes as a function of d_{Cu} are seen; that is, a nonmonotonic temperature dependence of $|J_{\text{inter}}|$. The temperature dependence for AFM coupling is larger than that for FM. This nonmonotonic behavior clearly indicates that the coupling between spin-wave modes will be more important for the *temperature dependence* of $|J_{\text{inter}}|$, than the smearing of the Fermi edge.

In conclusion, the strength of the effective $T^{3/2}$ dependence of J_{inter} depends on various parameters of the electronic band structure, electron–hole excitations, and spin-wave excitations. Further *in situ* FMR experiments with different Cu thickness and full angular- and temperature-dependent measurements will give the key information to understand the IEC. Recent quantum mechanical calculations based on an extended Heisenberg model give clear evidence that magnon excitations are responsible for about 75% of the temperature dependence of the IEC. The remaining 25% is due to temperature effects in the effective quantum well, formed by the spacer and the spacer/magnet interfaces like

reduced spin asymmetry or softening of the spacer Fermi surface (Schwieger *et al.*, 2007).

Finally, we come back to Figure 6(c) where the Weinberger group has calculated layer resolved the K anisotropy (ΔE_B) and the IEC for an $\text{Ni}_8/\text{Cu}_d/\text{Ni}_9$ trilayer. We see that the anisotropy energy depends strongly on the c/a ratio as discussed in the previous section. We also notice that for $d_{\text{Cu}} = 3$ ML and $d_{\text{Cu}} = 9$ ML the spacer does not contribute to the MAE. The layer-resolved calculated IEC demonstrates clearly that more or less only the Ni layer contributes to the exchange coupling directly at the interface but for very thin spacers (3 ML) the Cu also makes a finite contribution.

4 DYNAMICS IN THE FMR, THE LINEWIDTH ΔH

Starting from Figure 1 it is obvious that the linewidth in the EPR and FMR is a measure of the spin relaxation, scattering, and spin fluctuations. Two principal relaxation paths are discussed in standard literature: spin–lattice relaxation and spin–spin relaxation. The former is a process in which energy dissipates from the magnetic system to the thermal bath. For the latter, energy is scattered within the magnetic spin system. It depends on the concentration of magnetic moments (dilute ferromagnets) and can be discussed in the framework of spin-wave excitations, magnon–magnon scattering, Stoner excitations, and so on. For both processes, phase transitions (structural or magnetic) are of importance: diverging spin fluctuations as a function of temperature will influence the linewidth. Müller and coworkers have given a nice example for the EPR: SrTiO_3 undergoes a structural phase transition at ≈ 105 K. If this crystal is doped with a paramagnetic center, the EPR will show a dramatic divergence of the linewidth at this phase-transition temperature (von Waldkirch *et al.*, 1973). Similar effects were observed for the classical antiferromagnet MnF_2 at the Néel temperature of $T_N = 67$ K (Burgiel and Stranberg, 1964). In both cases, a dramatic divergence of ΔH is observed.

For bulk ferromagnets like Ni and Fe whiskers also a line broadening in the FMR occurs starting from low temperature and approaching the Curie temperature from the T_C^- side.

On the right-hand part of Figure 8, the FMR linewidth $\Delta H(T)$ is shown for bulk Ni. A very sharp peak of only 7 K width is measured at the Curie temperature of $T_C \approx 630$ K. The line broadens from below 200 Oe to more than 1.6 kOe. How can this be understood? Approaching the phase transition from the T_C^- side, one observes a breakdown of the uniform precession of the magnetization. The uniform rotation of the spin waves with infinite wavelength breaks into pieces because of thermal excitations. This increases the FMR

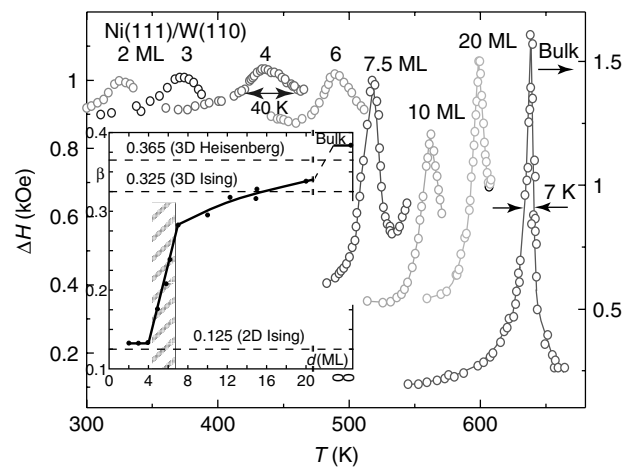


Figure 8. FMR linewidth $\Delta H(T)$ of bulk and ultrathin Ni films $d = 2$ – 20 ML as a function of the temperature. Note the very sharp peak for thicker films and the very broad peak for the ultrathin 2D film. The inset shows the critical exponent β and the transition 3D \rightarrow 2D. For details see Li and Baberschke (1992).

linewidth. Starting from the paramagnetic side above T_C^+ also a narrow line of 250 Oe width is observed. The susceptibility and spin–spin correlation length ξ increase dramatically owing to Gaussian and critical fluctuations. The sharpness of the peak in the linewidth is surprising. It depends very much on the high perfection of the crystallographic structure of the single crystal. (Since these measurements are performed in an external magnetic field, ξ will not diverge to infinite.) Applying the UHV-FMR to Ni(111) thin films grown on W(110), we observe in the first place a shift of the diverging peak to lower temperature in full agreement with the thickness-dependent Curie temperature of ultrathin films caused by *finite size* effects (Baberschke, 1996). At a certain thickness of $d = 4$ – 6 ML, the Ni film undergoes a transition from 3D to 2D behavior. Immediately, we observe a broadening of the linewidth peak as indicated by ~ 40 K in the figure. This can be easily understood because the fluctuations in less than 3D are enhanced and extended over a larger range of temperature. For details see (Li and Baberschke, 1992; Li *et al.*, 1990).

4.1 Gilbert damping and magnon–magnon scattering

In the following text we focus on the analysis of the linewidth in FMR experiments in ultrathin films deep in the ferromagnetic phase $T \ll T_C$. This is of particular importance for the investigation of magnetization dynamics and magnetization reversal in magnetic nanostructures. The commonly used ansatz is to add the so-called Gilbert

damping to the equation of motion, equation (2), that is, the second term in equation (11). This Landau–Lifshitz–Gilbert (LLG) equation has been discussed in great detail in many review articles. For FMR in bulk material see, for example (Sparks, 1964; Vonsovskii, 1966), for ultrathin films see, for example (Heinrich, 1994, 2005). The Gilbert ansatz is based on a double vector product $-\vec{M} \times (\vec{M} \times \vec{H}_{\text{eff}})$ as shown in Figure 9(b) with a resulting vector that is always pointing toward the symmetry axis of the Larmor precession. For small angles β between \vec{H}_{eff} and \vec{M} , this can be approximated by the time derivative $\partial \vec{M} / \partial t$.

$$\frac{\partial \vec{M}}{\partial t} = -\gamma(\vec{M} \times \vec{H}_{\text{eff}}) + \frac{G}{\gamma M_S^2} \left[\vec{M} \times \frac{\partial \vec{M}}{\partial t} \right] \quad \text{with} \quad \alpha = G/\gamma M \quad (11)$$

Thus it can be interpreted as a velocity-proportional viscous damping like in mechanical (Stokes) friction. The viscosity damps the Larmor precession, and the magnetization spirals into the z axis pointing to the surface of a sphere, that is, the length of \vec{M} stays constant but the expectation value $\langle M_z \rangle$ increases if $\beta \rightarrow 0$. This is indicated in Figure 9(b) as relaxation path 1. A uniform motion of the magnetization plus a viscous damping leads to a dissipation of energy into the thermal bath (path 1 in Figure 9(a) – an irreversible process. Two notations are commonly used in equation (11): (i) G , the Gilbert-damping parameter, given as a relaxation rate in s^{-1} , or (ii) the dimensionless parameter α in analogy to the viscous damping. The relaxation rate per second G seems to be more instructive for easier comparison with other relaxation rates in the literature. As discussed in Section 2, standard EPR/FMR experiments use a fixed microwave frequency and scan the external Zeeman field H_0 . Under these

conditions, the LLG (11) leads to a linewidth ΔH_G depending linearly [4] on ω

$$\Delta H_G(\omega) \approx \frac{2}{\sqrt{3}} \frac{G}{\gamma^2 M} \frac{\omega}{\cos \beta} \quad (12)$$

One example is shown in Figure 3 in which for 1 GHz experiments the linewidth for a 10 ML Ni film is very narrow in the range of 10–20 Oe, whereas for the most commonly used 10 GHz frequency the linewidth increases up to 200–250 Oe.

A second relaxation process is discussed in standard literature and indicated in Figure 9(c): The uniform motion of the magnetization (or switching the magnetization) may scatter into excited states of the magnetic subsystem (spin waves, Stoner excitations, magnon–magnon scattering, etc.) The projection of \vec{M} onto the z axis stays constant since the precessional energy is scattered into the transverse components M_x and M_y . (For details see Sparks, 1964). These processes may be reversible and are indicated in Figure 9(a) as path 2. They are in full analogy with optical spectroscopy. In the long run, these excitations will also decay into the thermal bath as indicated by path 3. One may raise the question: Is there any experimental evidence for the appearance of this second relaxation process, that is, scattering within the magnetic subsystem, in magnetic nanostructures? The theoretical background to study this question is known for a long time. One possible model is described by the Bloch–Bloembergen equation (Bloembergen, 1950; Bloch, 1946)

$$\frac{\partial \vec{M}}{\partial t} = -\gamma(\vec{M} \times \vec{H}_{\text{eff}}) - \frac{M_x}{T_2} \hat{e}_x - \frac{M_y}{T_2} \hat{e}_y - \frac{M_z - M_S}{T_1} \hat{e}_z \quad (13)$$

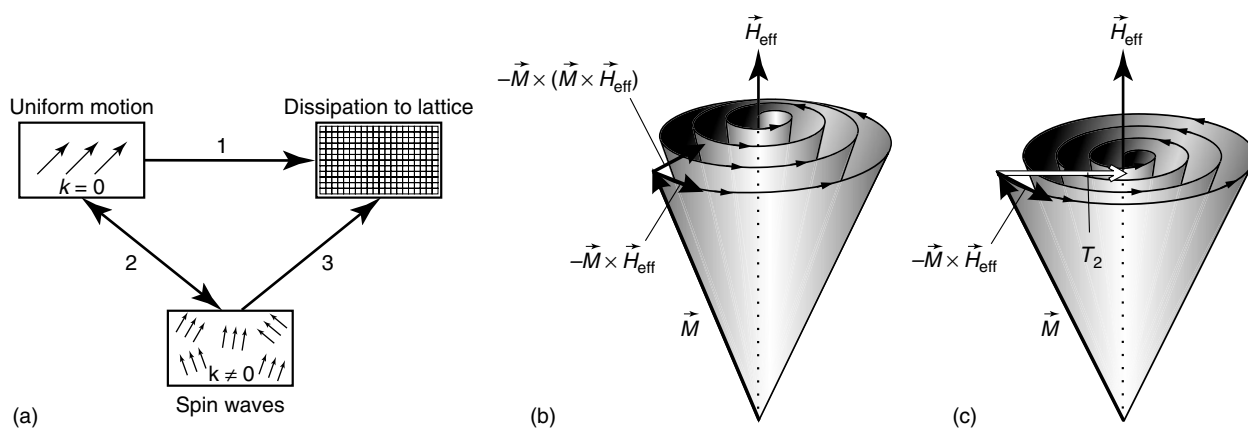


Figure 9. Schematic illustration of different relaxation processes taken from Suhl (1998); Sparks (1964): (a) The uniform motion of the magnetization with $k = 0$ in an FMR experiment may scatter with energy dissipation into the thermal bath (path 1). In path 2 it can also scatter into spin waves with $k \neq 0$ – a reversible process. In the long run, this energy also travels along path 3 into the heat sink. (b) Depicts the LLG scenario from equation (11). (c) Shows the Bloch–Bloembergen process for spin–spin relaxation.

In this case, two different relaxation rates are introduced into the equation of motion (Abragam and Bleaney, 1966): the longitudinal relaxation rate T_1 , that is, the direct path into the thermal bath, and the so-called transverse rate, T_2 , by which energy is scattered into the transverse magnetization components M_x and M_y . This is depicted in Figure 9(c). The projection of \vec{M} on the effective field \vec{H}_{eff} stays constant and energy is scattered into the transverse components M_x and M_y . This is a dephasing of the former coherent rotation of the magnetization as discussed in the previous section. This scenario of a transverse relaxation rate is known, for example, Sparks (1964); Mills and Rezende (2003); Suhl (1998). Only very recently, Arias and Mills have calculated this type of magnon–magnon scattering in a quantitative manner for standard FMR experiments in ultrathin films (Arias and Mills, 1999, 2000) (see also **Spin Waves: History and a Summary of Recent Developments, Volume 1**). The result for the FMR linewidth is given below, with Γ as a parameter

$$\Delta H_{2M}(\omega) = \Gamma \sin^{-1} \frac{\sqrt{\omega^2 + (\omega_0/2)^2} - \omega_0/2}{\sqrt{\omega^2 + (\omega_0/2)^2} + \omega_0/2} \quad (14)$$

It is obvious that the frequency dependence of the linewidth for magnon–magnon scattering is by no means linear. It saturates at very high frequency and starts with a steep slope at low frequencies (Figure 10). The first experimental evidence of a nonlinear $\Delta H(\omega)$ was reported for Fe/V nanostructure in Lindner *et al.* (2003) and for Fe/GaAs films, (Woltersdorf and Heinrich, 2004). Recently, the FMR linewidth of Fe/V multilayers has been measured

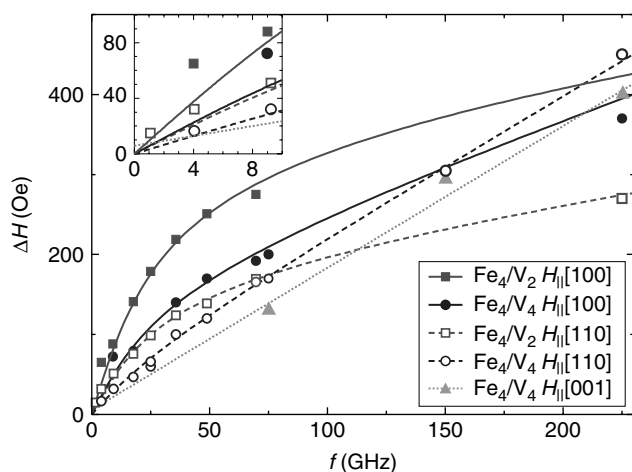


Figure 10. FMR linewidths of two Fe/V-multilayer samples for different in-plane and out-of-plane orientations of the external field as a function of the microwave frequency. The inset is a magnification of the low frequency regime. For details see Lenz *et al.* (2006).

and analyzed over a very large frequency range from 1 to 225 GHz as shown in Figure 10 (Lenz *et al.*, 2006). Key information can be obtained from Figure 10: (i) FMR measurements at very low frequencies (1–4 GHz) unambiguously show that the linewidth narrows dramatically, that is to say ΔH is given by relaxation processes only. A practice used in the literature for earlier experiments between 9 and 36 GHz to *assume* a linear frequency dependence (Celinski and Heinrich, 1991), extrapolating from this, an apparent residual linewidth (the tangent crossing the y axis) does not always seem to be justified. (ii) For all in-plane orientations of the external field ([001] and [110]), one observes a nonlinear frequency dependence. In contrast, for \vec{H} normal to the film plane ([001], full triangles), a 100% linear frequency dependence is observed. This is in perfect agreement with the theoretical prediction in (Arias and Mills, 1999, 2000). The authors of (Lenz *et al.*, 2006) deduce a constant (independent of orientation) Gilbert damping of $\sim 0.7 \times 10^8 \text{ s}^{-1}$ for these multilayers. Fitting equation (14) to the curved frequency dependence yields a magnon–magnon scattering rate of $\gamma\Gamma \approx 10\text{--}50$ larger than the Gilbert damping. Thus, experimental evidence is given that both relaxation mechanisms (longitudinal and transverse scattering) are active in magnetic nanostructures. A combination of magnon–magnon scattering, modeled by equations (13) and (14), and a viscous Gilbert damping described by equations (11) and (12) seems to give a better insight into the spin dynamics of ultrathin films. For the particular investigated systems, Fe/V multilayers and Fe films on GaAs, the magnon–magnon scattering of $1/T_2 \approx 10^9 \text{ s}^{-1}$ seems to be about 2 orders of magnitude faster than the viscous Gilbert damping of $1/T_1 \approx 10^7 \text{ s}^{-1}$.

4.2 Spin-pump effects in the FMR

Consider in Figure 11(a) that 3d magnetic moments of the FM are excited by a microwave radiation $h\nu$ and undergo a Larmor precession in an external field, equations (1) and (2). It is standard textbook reasoning that the local 3d moments are coupled to the sea of conduction electrons via the classical s – d exchange interaction. In turn, the conduction band of the FM is hybridized with the conduction band of the NM. This classical s – d exchange between spin waves and s electrons has been used by Janossy and coworkers (Silsbee *et al.*, 1979; Monod and Janossy, 1977) to activate and enhance the Larmor precession in the NM conduction band, the so-called conduction electron spin resonance (CESR). Angular momentum is transferred to the conduction band and then transported into the NM. These authors used highest-purity Au as NM and were able to detect the spin current of the Au conduction band through micrometer thick Au. This has been monitored at the right-hand end of Figure 11(a) either as emitted

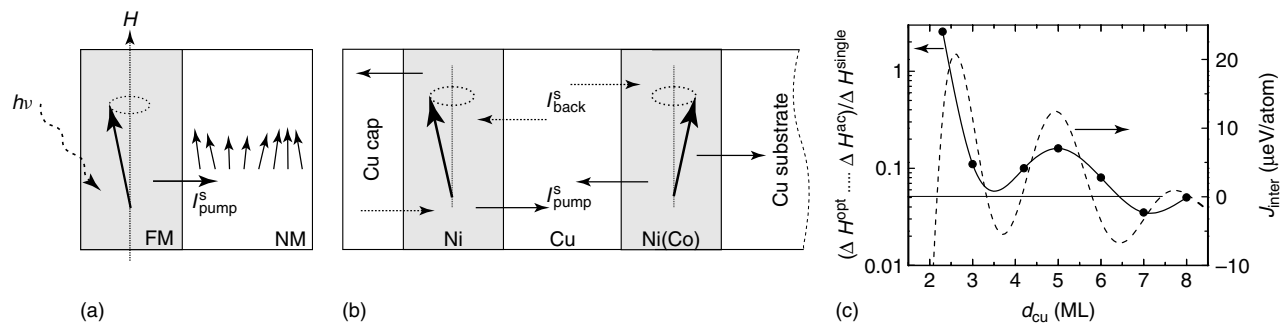


Figure 11. Schematic illustration of the spin-pump effect of (a) a single interface and (b) a trilayer consisting of two different ferromagnetic films and a nonmagnetic spacer. (c) Oscillatory behavior of the linewidth as a function of the Cu spacer. The data are taken from Lenz *et al.* (2004) for a $\text{Ni}_8/\text{Cu}_x/\text{Ni}_9$ trilayer.

microwave radiation or by exciting another magnetic system. This is the basic mechanism called *spin pumping* in our days. Thus, angular momentum and energy are lost from the ferromagnetic film and transported to the NM (metal, semiconductor). In the frame of Figure 9(a), this can be seen as a dissipation of energy like path 1 in Figure 9(a). Recently, such a mechanism became of particular interest for magnetic nanostructures consisting of two ferromagnetic films separated by an NM spacer, see Figure 11(b). Such a scenario has been investigated theoretically in Tserkovnyak *et al.* (2002) and by others. Experimental evidence was given in Heinrich *et al.* (2003) for Fe/40 ML Au/Fe (see also **Magnetic Ultrathin Films, Volume 4**). The thickness of the spacer will be of particular interest. For a larger thickness, like 40 ML Au, there is no IEC between FM1 and FM2 – see Section 3.3. Only ballistic transport is possible for the spin current depending on the perfection of the spacer and its interfaces. For ultrathin spacer films of only a few monolayers, one expects also some IEC (see Section 3.3) influencing the FMR linewidth. Constructive or destructive interference phenomena and quantum well effects should be detectable in the spin current I_{pump}^s . In Section 3.3 we have seen that a trilayer consisting of two different ferromagnets (Ni and Co or two Ni films with different thickness) has two different (acoustic and optic) FMR modes. In Lenz *et al.* (2004) and Heinrich *et al.* (2003) first evidence is given that indeed the FMR linewidths influence each other when both resonance conditions coincide. Figure 11(c) shows the difference between the optic and acoustic linewidth $\Delta H^{\text{opt}} - \Delta H^{\text{ac}}$ for $\text{Ni}_8/\text{Cu}_x/\text{Ni}_9$ with an ultrathin spacer thickness of $d_{\text{Cu}} = 2\text{--}8$ ML. On the left-hand side, the relative change in the linewidth normalized to the linewidth for a single film is plotted on a logarithmic scale, whereas on the right-hand side the energy scale for J_{inter} (dashed line) is shown. The broadening of the optical linewidth is the largest (more than a factor of 2) for the thinnest Cu spacer and the largest J_{inter} . A clear oscillatory behavior for both linewidth and J_{inter} is observed as a function of d_{Cu} .

5 SUMMARY, OUTLOOK

As discussed by several examples, microwave spectroscopy is a very useful technique to investigate ultrathin ferromagnetic films. It covers the ferromagnetic as well as the paramagnetic regime. It is sensitive to ferromagnetic as well as antiferromagnetic IEC in superstructures. The static resonance conditions, its angular and temperature dependence as well as the linewidth, yield reliable information on the static and dynamic parameters of ultrathin film magnetism. If the standard FMR technique is combined with state-of-the-art surface science and UHV technique, the combined UHV-FMR spectroscopy opens a new challenging research field to study the growth and crystallographic modifications, the electronic band structure, and the direct observation of the magnetism in one experiment. Such a complete set of experimental observables is the best input for a better theoretical description of the magnetism of magnetic nanostructures. Standard FMR technique might have one drawback: the spectroscopy has no spatial resolution. The wavelength of the microwave ranges from submillimeters to a few centimeters and the absorbed energy out of the microwave radiation is the macroscopic response of the whole specimen. A recent development to overcome this problem is to combine an STM or AFM tip with FMR. Several groups have developed this technique. A lateral resolution in the range of 10–100 nm was reached (Meckenstock *et al.*, 2003; Meckenstock *et al.*, 2004). Another interesting new development is the combination of synchrotron radiation and FMR. XMCD has the advantage of being element specific. XMCD also has access to orbital and spin magnetic moments. If this can be used to probe the change in the magnetization induced by the precession of magnetic moments, this X-ray-detected magnetic resonance (XDMR) is the analogue of the well-known optical-detected magnetic resonance (ODMR). First experimental results at the *K*-edge of Fe in a YIG crystal have been reported recently (Goulon *et al.*, 2005). Also, the

combination of an electronic network analyzer with FMR spectroscopy offers the possibility of studying the dynamics of magnetic nanostructures in the frequency as well as in the time (pulsed) domain (Council *et al.*, 2004).

Finally we point out recent advances in the theory of the FMR in ultrathin films: The vast majority uses a classical continuum model to interpret experimental spectra, where the classical LLG equation of motion for the magnetization or an expansion of the free energy is considered. Recently a microscopic Heisenberg Hamiltonian was used to directly calculate for FMR the spin-wave resonance modes and external resonance fields as a function of the field direction and as a function of temperature (Schwieger *et al.*, 2005). Future work will provide better microscopic insight into the FMR of ultrathin films.

NOTES

- [1] The FMR community uses a positive γ value, whereas in EPR the negative sign of the charge is taken into account.
- [2] Note that many other experimental techniques like MOKE, spin-polarized PE, and so on, measure the magnetization in arbitrary units, only. MAE and IEC, for example, measured by FMR are given in absolute energy units per particle. These numbers are of interest for comparison with theory.
- [3] This equation is strictly valid only for g -values close to two.
- [4] Note that this linear frequency dependence is a consequence of the field-scanning technique in conventional FMR. For other experimental techniques at fixed magnetic field and scanning the microwave frequency or for Brillouin light scattering the analysis of the measured linewidth is different, see (Mills and Rezende, 2003). Caution has to be taken when comparing different experiments.

ACKNOWLEDGMENTS

The idea of EPR and FMR in metals and its combination with UHV technique was brought to our attention by S. Hufner (FUB) and R. Orbach (UCLA). Discussions with H. Ebert, M. Farle, K. Lenz, J. Lindner, D.L. Mills, and R.Q. Wu are acknowledged. Special thanks is given to C. Sorg, E. Kosubek, and K. Lenz for their assistance in the preparation of the manuscript. Financial support was given over decades by the Deutsche Forschungsgemeinschaft DFG under the research grants Sfb 161, Sfb 6, and Sfb 290.

REFERENCES

- Abragam, A. and Bleaney, B. (1966). *Electron Paramagnetic Resonance of Transition Ions*, Clarendon Press Oxford.
- Aharoni, A. (2000). *Introduction to the Theory of Ferromagnetism*, Oxford University Press.
- Anisimov, A.N., Farle, M., Pouloupoulos, P., *et al.* (1999). Orbital magnetism and magnetic anisotropy probed with ferromagnetic resonance. *Physical Review Letters*, **82**, 2390.
- Antoniak, C., Lindner, J., Farle, M., *et al.* (2005). Magnetic anisotropy and its temperature dependence in iron-rich $\text{Fe}_x\text{Pt}_{1-x}$ nanoparticles. *Europhysics Letters*, **70**, 250.
- Arias, R. and Mills, D.L. (1999). Extrinsic contributions to the ferromagnetic resonance response of ultrathin films. *Physical Review B*, **60**, 7395.
- Arias, R. and Mills, D.L. (2000). Extrinsic contributions to the ferromagnetic resonance response of ultrathin films. *Journal of Applied Physics*, **87**, 5455.
- Baberschke, K. (1976). Electron spin resonance in superconducting materials. *Zeitschrift fur Physik B*, **24**, 53.
- Baberschke, K. (1996). The magnetism of nickel monolayers. *Applied Physics A*, **62**, 417.
- Baberschke, K. (2001). *Band-Ferromagnetism*, Vol. 580, p. 27 *Lecture Notes in Physics*, Springer: Berlin.
- Baberschke, K. and Tsang, E. (1980). The Kondo-effect on the paramagnetic resonance of dilute Au:Yb. *Physical Review Letters*, **45**, 1512.
- Berghaus, A., Farle, M., Li, Yi., *et al.* (1989). Absolute determination of the magnetic anisotropy of ultrathin Gd and Ni/W(110). *Proceedings in Physics*, **50**, 61.
- Bloch, F. (1946). Nuclear Induction. *Physical Review*, **70**, 460.
- Bloembergen, N. (1950). On the ferromagnetic resonance in nickel and supermalloy. *Physical Review*, **78**, 572.
- Brewer, W.D., Scherz, A., Sorg, C., *et al.* (2004). Direct observation of orbital magnetism in cubic solids. *Physical Review Letters*, **93**, 077205.
- Bruno, P. (1995). Theory of interlayer magnetic coupling. *Physical Review B*, **52**, 411.
- Bruno, P. and Chappert, C. (1991). Oscillatory coupling between ferromagnetic layers separated by a nonmagnetic metal spacer. *Physical Review Letters*, **67**, 1602.
- Burgiel, J.C. and Stranberg, M.W.P. (1964). Antiferromagnetic resonance linewidth in MnF_2 near the transition temperature. *Journal of Applied Physics*, **35**, 852.
- Celinski, Z. and Heinrich, B. (1991). Ferromagnetic resonance linewidth of Fe ultrathin films grown on a bcc Cu substrate. *Journal of Applied Physics*, **70**, 5935.
- Coqblin, B. (1977). *The Electronic Structure of Rare-Earth Metals and Alloys*, Academic Press: London.
- Council, G., Kim, J-V., Shigeto, K., *et al.* (2004). Inductive measurement of the high frequency permeability of a Permalloy thin film. *Journal of Magnetism and Magnetic Materials*, **272**, 290.
- Farle, M. (1998). Ferromagnetic resonance of ultrathin metallic layers. *Reports on Progress in Physics*, **61**, 755.

- Farle, M. and Baberschke, K. (1987). Ferromagnetic order and the critical exponent γ for a Gd monolayer. An ESR-study. *Physical Review Letters*, **58**, 511.
- Farle, M., Platow, W., Kosubek, E., *et al.* (1999). Magnetic anisotropy of Co/Cu(111) ultrathin films. *Surface Science*, **439**, 146.
- Farle, M., Zomack, M., Baberschke, K., *et al.* (1985). ESR of adsorbates on single crystal metal surfaces under UHV conditions. *Surface Science*, **160**, 205.
- Gambardella, P., Rusponi, S., Veronese, M., *et al.* (2003). Giant magnetic anisotropy of single cobalt atoms and nanoparticles. *Science*, **300**, 1130.
- Goulon, J., Rogalev, A., Wilhelm, F., *et al.* (2005). X-ray detected magnetic resonance at the Fe K-edge in YIG: forced precession of magnetically polarized orbital components. *JETP LETTERS*, **82**(11), 696–701.
- Hammerling, R., Zablouil, J., Weinberger, P., *et al.* (2003). Interlayer exchange coupling and magnetic anisotropy in prototype trilayers: Ab initio theory versus experiment. *Physical Review B*, **68**, 092406.
- Heinrich, B. (1994). *Ultrathin Magnetic Structures II*, Springer-Verlag: Berlin.
- Heinrich, B. (2005). *Ultrathin Magnetic Structures III*, Springer: Berlin Heidelberg New York.
- Heinrich, B., Tserkovnyak, Y., Woltersdorf, G., *et al.* (2003). Dynamic exchange coupling in magnetic bilayers. *Physical Review Letters*, **90**, 187601.
- Heinrich, B., Urquhart, K.B., Arrott, A.S., *et al.* (1987). Ferromagnetic-resonance study of ultrathin bcc Fe(100) films grown epitaxially on fcc Ag(100) substrates. *Physical Review Letters*, **59**, 1756.
- Hjortstam, O., Baberschke, K., Wills, J.M., *et al.* (1997). Magnetic anisotropy and magnetostriction in tetragonal and cubic Ni. *Physical Review B*, **55**, 15026.
- Huang, F., Mankey, G.J., Willis, R.F., *et al.* (1994). Interfacial anisotropy and magnetic transition of cobalt films on Cu(111). *Journal of Applied Physics*, **75**, 6406.
- Kohlhepp, J., Elmers, H.J., Gradmann, U., *et al.* (1993). Magnetic interface anisotropies of Co/Cu(111) and Co/Au(111) interfaces from ultrathin Co films on Cu(111). *Journal of Magnetism and Magnetic Materials*, **121**, 483.
- Lenz, K., Tolinski, T., Lindner, J., *et al.* (2004). Evidence of spin-pumping effect in the ferromagnetic resonance of coupled trilayers. *Physical Review B*, **69**, 144422.
- Lenz, K., Wende, H., Kuch, W., *et al.* (2006). Two-magnon scattering and viscous Gilbert damping in ultrathin ferromagnets. *Physical Review B*, **73**, 144424.
- Li, Y. and Baberschke, K. (1992). Dimensional crossover in ultrathin Ni(111) films on W(110). *Physical Review Letters*, **68**, 1208.
- Li, Y., Farle, M., Baberschke, K., *et al.* (1990). Critical spin fluctuations and curie temperatures of ultrathin Ni(111)/W(110): a magnetic-resonance study in ultrahigh vacuum. *Physical Review B*, **41**, 9596(R).
- Lindner, J. and Baberschke, K. (2003a). Ferromagnetic resonance in coupled ultrathin films. *Journal of Physics: Condensed Matter*, **15**, S465.
- Lindner, J. and Baberschke, K. (2003b). In situ ferromagnetic resonance: an ultimate tool to investigate the coupling in ultrathin magnetic films. *Journal of Physics: Condensed Matter*, **15**, R193.
- Lindner, J., Lenz, K., Kosubek, E., *et al.* (2003). ‘Non-Gilbert-type’ damping of the magnetic relaxation in ultrathin ferromagnets: importance of magnon-magnon-scattering. *Physical Review B*, **68**, 060102(R).
- Lindner, J., Rüdert, C., Kosubek, E., *et al.* (2002). $T^{3/2}$ -dependence of the interlayer exchange coupling in ferromagnetic multilayers. *Physical Review Letters*, **88**, 167206.
- Meckenstock, R., Rastei, M.V., Bucher, J.P., *et al.* (2004). Local magnetoresistance and ferromagnetic resonance measurements with a sliding probe contact. *Journal of Applied Physics*, **95**, 6753.
- Meckenstock, R., Spoddig, D., Dietzel, D., *et al.* (2003). Scanning thermal microwave resonance microscopy of Ni nanodots. *Review of Scientific Instruments*, **74**, 789.
- Meyer, A.J.P. and Asch, G. (1961). Experimental g and g values of Fe, Co, Ni, and their alloys. *Journal of Applied Physics*, **32**, 330S.
- Mills, D.L. and Rezende, S.M. (2003). *Spin Dynamics in Confined Magnetic Structure II*, Vol. 87, *Topics in Applied Physics*, Springer: Berlin.
- Monod, P. and Janossy, A. (1977). Conduction electron spin resonance in Au. *Journal of Low Temperature Physics*, **26**, 311.
- Nagel, J., Baberschke, K., Tsang, E., *et al.* (1980). ESR of Er^{3+} and Yb^{3+} in gold between 100 mK and 1 K. *Journal of Magnetism and Magnetic Materials*, **15–18**, 730.
- Ney, A., Lenz, K., Pouloupoulos, P., *et al.* (2002). Absolute magnetometry on ultrathin 3d-metal films by UHV-SQUID. *Journal of Magnetism and Magnetic Materials*, **240**, 343.
- Orton, J.W. (1968). *Electron Paramagnetic Resonance*, Iliffe Books LTD: London.
- Pake, G.E. (1962). *Paramagnetic Resonance*, W A Benjamin: New York.
- Scherz, A., Wende, H., Pouloupoulos, P., *et al.* (2001). Induced V and reduced Fe moment at the interface of Fe/V(001) superlattices. *Physical Review B*, **64**, 180407(R).
- Schulz, B. and Baberschke, K. (1994). Crossover from in-plane to perpendicular magnetization in ultra thin Ni/Cu(001) films. *Physical Review B*, **50**, 13467.
- Schwieger, S., Kienert, J., Lenz, K., *et al.* (2007). Magnetic excitations: the main source of the temperature dependence of IEC in nanostructures. *Physical Review Letters*, **98**, 057205.
- Schwieger, S., Kienert, J., Nolting, W., *et al.* (2005). Temperature dependence of interlayer exchange coupling: spin waves versus spacer effects. *Physical Review B*, **71**, 174441.
- Schwieger, S. and Nolting, W. (2004). Origin of the temperature dependence of interlayer exchange coupling in metallic trilayers. *Physical Review B*, **69**, 224413.
- Silsbee, R.H., Janossy, A., Monod, P., *et al.* (1979). Coupling between ferromagnetic and conduction-spin-resonance modes at a ferromagnetic normal-metal interface. *Physical Review B*, **19**, 4382.
- Smit, J. and Beljers, H.G. (1955). Ferromagnetic resonance absorption in $\text{BaFe}_{12}\text{O}_{19}$, a highly anisotropic crystal. *Philips Research Report*, **10**, 113.

- Sparks, M. (1964). *Ferromagnetic-Relaxation Theory, Advanced Physics Monograph Series*, McGraw-Hill: New York.
- Stearns, M. (1986). *Landolt Börnstein: Magnetic Properties of Metals*, Springer: Berlin, Vol. III/19a.
- Stetter, U., Farle, M., Baberschke, K., *et al.* (1992). Critical behavior of strained epitaxial Gd films: in situ ac-susceptibility measurements in UHV. *Physical Review B*, **45**, 503.
- Suhl, H. (1998). Theory of the magnetic damping constant. *IEEE Transactions on Magnetics*, **34**, 1834.
- Tserkovnyak, Y., Brataas, A., Bauer, G.E.W., *et al.* (2002). Spin pumping and magnetization dynamics in metallic multilayers. *Physical Review B*, **66**, 224403.
- Uiberacker, C., Zablouil, J., Weinberger, P., *et al.* (1999). Lattice relaxation driven reorientation transition in Ni_n/Cu(100). *Physical Review Letters*, **82**, 1289.
- Vonsovskii, S.V. (1966). *Ferromagnetic Resonance*, Pergamon Press: Oxford London.
- Vonsovskii, S.V. (1974). *Magnetism*, Wiley: New York.
- von Waldkirch, T., Müller, K.A., Berlinger, W., *et al.* (1973). Fluctuations in SrTiO₃ near the 105-K phase transition. *Physical Review B*, **7**, 1052.
- White, R.M. (1970). *Quantum Theory of Magnetism*, McGraw-Hill Book Company.
- Woltersdorf, G. and Heinrich, B. (2004). Two-magnon scattering in a self-assembled nanoscale network of misfit dislocations. *Physical Review B*, **69**, 184417.
- Zomack, M. and Baberschke, K. (1986). Electron Spin Resonance study on NO₂ adsorbed on Kr/Ag(110) at 20 K. *Surface Science*, **178**, 618.

APPENDICES

A UNITS

The history of ferromagnetism and magnetic anisotropy went different routes and was uncoupled from other areas of solid-state magnetism, unfortunately. As a consequence, the classification of magnetic anisotropy contributions used an expansion different from Legendre polynomial expansion in crystal-field theory. Moreover, as a consequence various units are used in the historical part of magnetoelasticity, namely, erg cm⁻³ and erg cm⁻², that is to say energy per volume and area, respectively. Other parts of solid-state physics and, in particular, the theory prefers eV/atom, that is to say energy per particle (see also **Theory of Magnetocrystalline Anisotropy and Magnetoelasticity in Transition-metal Systems, Volume 1**). This newer notation started to be used in surface and thin-film magnetism and we strongly advocate it, since it facilitates communication with theory and gives an easier insight. For example, in thin-film magnetism Fe, Co, and Ni ions contribute equally strongly to the anisotropy energy, be it a surface atom or an atom in the inner part of a nanostructure, namely, 10–100 μeV/atom. In the older version it would read 1.5–15 × 10⁶ ergcm⁻³ for K^v and 0.03–0.3 × 10⁶ ergcm⁻² for K^s , which is not so easy to compare. A transformation of the older into the newer notation is simply given by the atomic volume of the individual elements, for example, for fcc Ni, 10⁶ ergcm⁻³ corresponds to 6.83 μeV/atom or 7.38 μeV/atom for bcc Fe, respectively.

B NOTATION OF THE MAGNETIC ANISOTROPY ENERGY

The magnetic part of the free-energy density and its anisotropy in ultrathin ferromagnetic films has only two origins: (i) the dipole–dipole interaction, which depends on M and the shape of the specimen, (ii) all other contributions

(crystalline MAE, magnetoelastic MAE, etc.) are caused by spin-orbit interaction or even better by a full relativistic treatment of the free-energy density. We recall that the exchange interaction $\vec{s}_1 \cdot \vec{s}_2$, the Heisenberg Hamiltonian, is completely isotropic, its energy levels do not depend on the direction in space in which the crystal is magnetized (Aharoni, 2000). The so-called anisotropic exchange is nothing but the anisotropy of the orbital magnetism projected to an effective spin space.

1. The dipole contribution: Mostly, a homogeneous dipole density is assumed with a dipolar field of $4\pi M$ and an energy density of $2\pi M^2$. For ultrathin films of a few monolayers only, this may not be completely appropriate. The dipolar field of a discrete lattice sum has been discussed elsewhere (Farle, 1998; Heinrich *et al.*, 1987). The discrete sum of point dipoles delivers somewhat smaller values for the dipolar contribution but this may even be an underestimation because it is currently clear that for 3d or 4f ferromagnets a finite distribution of the magnetic moment density has been measured by means of neutron scattering. In conclusion, if the continuous dipole density ansatz is inadequate for magnetic monolayers or nanometer dots, the real value will be somewhat smaller but not as small as calculated from a lattice grid with point dipoles.
2. Spin-orbit effects: The experimentalist measures the total (or effective) magnetic anisotropy field or energy. Subtracting from this measured value a separately determined or calculated dipolar contribution, the remaining part is given by the spin-orbit-caused contribution and is commonly labeled with K_i . We do not advise to analyze the sum of the two contributions with K_{eff} because the temperature dependence of the dipolar contribution and the spin-orbit-caused anisotropy may be completely

different. The latter contribution, which is also called ΔE_{band} in the *ab initio* theory, is calculated from the band structure. It has anisotropic contributions in various spacial directions of the ferromagnet. To facilitate a comparison between different experimental results or comparison to theoretical *ab initio* calculations we list below different notations. Owing to the pseudomorphic growth of ultrathin Fe, Co, Ni, and Gd films on cubic substrate crystals, one hardly has cubic symmetry in the ultrathin film but rather structures of tetragonal or lower symmetry.

$$E_{\text{tetr}} = -K_2 \alpha_z^2 - \frac{1}{2} K_{4\perp} \alpha_z^4 - \frac{1}{2} K_{4\parallel} (\alpha_x^4 + \alpha_y^4) + \dots \quad (\text{A1a})$$

$$= -K_2 \cos^2 \theta - \frac{1}{2} K_{4\perp} \cos^4 \theta - \frac{1}{2} K_{4\parallel} \frac{1}{4} (3 + \cos 4\varphi) \sin^4 \theta + \dots \quad (\text{A1b})$$

$$= -K_2' \sin^2 \theta - K_{4\perp} \sin^4 \theta + K_{4\parallel} \cos 4\varphi \sin^4 \theta + \dots \quad (\text{A1c})$$

$$E_{\text{hex}} = K_2 \sin^2 \theta + \frac{1}{2} K_{2\parallel} \cos 2\varphi \sin^2 \theta + K_4 \sin^4 \theta + K_{6\perp} \sin^6 \theta + K_{6\parallel} \cos 6\varphi \sin^6 \theta + \dots \quad (\text{A2})$$

In the preceding equations, the free-energy density is expanded in terms of trigonometric functions. Equation (A1a) used by Heinrich (1994) is identical to equation (A1b), which is given as a function of polar and azimuthal angles up to fourth order. Quite often this energy is expanded

in a sine function with the same polar angle θ , given in equation (A1c). It is obviously clear that the prefactor K_2' of equation (A1c) is not identical to the one in equations (A1a) and (A1b) ($K_2' = K_2 + K_{4\perp}$). Also, the fourth-order contributions differ. Moreover, quite often the MAE is measured only in two directions: the easy and hard axes. The total energy difference is projected onto the second-order $\cos^2 \theta$ term – often labeled with K_u for uniaxial MAE. For a proper determination of the various energy contributions, a full angular-dependent measurement is required including the field-dragging effect if the external field H_0 is not aligned parallel to the easy or hard axes. It is well established for ultrathin films that the fourth-order term $K_{4\perp}$ is by no means small. Quite often it is in the same order of magnitude as K_2 . Less popular but maybe more instructive is the expansion of the free energy into spherical harmonics (Vonsovskii, 1974; Coqblin, 1977; Farle, 1998). Clearly, the terms with power \cos^n are grouped differently, resulting in different prefactors and their temperature dependence. For bulk ferromagnets the trigonometric expansion has been used mostly and the K_2 , K_4 , and K_6 contributions as a function of temperature are listed in the literature (Stearns, 1986). This temperature dependence with the oscillatory \pm values and zero crossings of the $K(T)$ parameters will change completely and look different if one expands the measured energy in terms of Legendre polynomials (Farle, 1998).

For ultrathin films of 5–10 atomic layers measured by FMR, for example, each of these K_i parameters can be decomposed into contributions of volume K_i^v and surface/interface K_i^s (Farle, 1998; Baberschke, 2001) following the reasoning by Néel.

$$K_i = K_i^v + 2K_i^s/d \quad (\text{A3})$$